PHYSICAL REVIEW B VOLUME 35, NUMBER 10 1 APRIL 1987

Experimental tests for the quantum behavior of a macroscopic degree of freedom: The phase difference across a Josephson junction

John M. Martinis,* Michel H. Devoret,* and John Clarke
Department of Physics, University of California, Berkeley, California 94720
and Materials and Molecular Research Division, Lawrence Berkeley Laboratory, Berkeley, California 94720
(Received 1 August 1986)

Experiments are described that demonstrate the quantum behavior of a macroscopic degree of freedom, namely the phase difference δ across a current-biased Josephson tunnel junction. The behavior of δ was deduced from measurements of the escape rate Γ of the junction from its zero-voltage state. The relevant parameters of the junction, that is, its critical current and shunting admittance, were determined *in situ* in the thermal regime from the dependence of Γ on bias current and from resonant activation in the presence of microwaves. It was found that the shunting capacitance was dominated by the self-capacitance of the junction while the shunting conductance was dominated by the bias circuitry. For an underdamped junction in the quantum regime, Γ became independent of temperature at low temperatures with a value that, with no adjustable parameters, was in excellent agreement with predictions for macroscopic quantum tunneling at $T=0$. When the critical current was reduced with a magnetic field so that the junction remained in the thermal regime at low temperatures, Γ followed the predictions of the thermal model, thereby showing the influence of extraneous noise to be negligible. In a further series of experiments, the existence of quantized energy levels in the potential well of the junction was demonstrated spectroscopically. The positions of the energy levels agreed quantitatively with quantum-mechanical predictions involving junction parameters measured in the thermal regime. The relative heights and widths of the resonances are in reasonable agreement with the predictions of a simple model.

I. INTRODUCTION

Do macroscopic degrees of freedom obey quantum mechanics? Until recently, the answer to this question was beyond the reach of experimentalists. Quantum mechanics survived at the macroscopic level only through collective phenomena such as superfluidity, superconductivity, flux quantization, or the Josephson effect. Although these phenomena are conventionally described as being "macroscopic," they are in fact manifestations on a macroscopic scale of the coherent addition of *microscopic* variables each governed by quantum mechanics. Leggett[1] has emphasized the importance of distinguishing macroscopic quantum phenomena originating in the superposition of a large number of microscopic variables from those displayed by a single macroscopic degree of freedom. This paper describes experiments on a system that, although it contains a large number of atomic constituents, is atomlike in the sense that it has such a single degree of freedom behaving quantum mechanically.

To observe quantum effects in a macroscopic system with a few degrees of freedom, one battles against the smallness of Planck's constant $\hbar$. There are two major requirements that the system must satisfy. First, the thermal energy must be sufficiently low to avoid incoherent mixing of eigenstates. Second, as analyzed in detail by Leggett,[1] the macroscopic degree of freedom must be sufficiently decoupled from other degrees of freedom for the lifetime of the quantum states to be long on the characteristic time scale of the system. To illustrate these requirements and to give an idea of the nature of a macroscopic quantum system we review briefly a simple, specific example first discussed by Leggett.

Consider a simple harmonic oscillator consisting of an inductor L threaded by a flux Φ and a capacitor C storing a charge Q. Because one needs to make observations on the system—for example, by means of leads connected to it—there is an inevitable coupling to the environment, which we represent by a resistor R in parallel with L and C; any losses in L or C are included in R. The resistor is in thermal equilibrium at temperature T: it both damps the circuit and provides a source of fluctuations.

Leaving aside the resistor for the moment, one can solve Schrödinger's equation exactly for the LC harmonic oscillator; the conjugate variables are Φ and Q, which are analogous to position and momentum. We define the natural angular frequency and impedance as $\omega_0=(LC)^{-1/2}$ and $Z_0=(L/C)^{1/2}$. To observe quantum effects the following inequalities must be satisfied: $\hbar\omega_0 \gg k_B T$ (no incoherent mixing of quantum states) and $R \gg Z_0$ (level width smaller than the level separation). Furthermore, to ensure there is only a single degree of freedom, that is, to avoid a multiplicity of cavity modes, we require the lumped-circuit approximation to be valid. Thus the circuit dimensions must be small compared with the wavelength $\omega_0/2\pi\bar{c}$, where $\bar{c}$ is the propagation velocity in the circuit. We note that in practice any line attached to the oscillator is likely to be many wavelengths long, and it appears to be difficult to construct such a line with a characteristic impedance Z_c greater than the impedance of free

space, 377 Ω; Z_c is typically 50 Ω.

To give a numerical example that should comfortably satisfy the conditions necessary to observe quantum effects we impose the constraints $\omega_0 > 10k_BT/\hbar$ and $Z_0 < Z_c/10 \approx 5$ Ω. For $T=10$ mK, we find $\omega_0/2\pi \gtrsim 2$ GHz. These estimates of ω_0 and Z_0 lead to $L \lesssim 350$ pH and $C \lesssim 15$ pH, values that are easily obtainable with standard photolithographic techniques. The ground-state energy is then $\hbar\omega_0/2 = (50 \text{ mK})k_B$, while the quantum-mechanical fluctuations in the ground state are the following:

$$\langle(\Delta\Phi)^2\rangle = \hbar Z_0/2 \approx 2.5\times10^{-34} \text{ Wb}^2 \approx [(8\times10^{-3})\Phi_0]^2$$

and

$$\langle(\Delta Q)^2\rangle = \hbar/2Z_0 \approx 10^{-35} \text{ C}^2 \approx (20e)^2 ,$$

where $\Phi_0 = h/2e$ is the flux quantum. It should be noted that the flux fluctuates quantum mechanically, but is not quantized in the usual sense of flux quantization.

Although it appears to be straightforward to fabricate a harmonic oscillator that will be in the quantum limit at routinely available temperatures, it is not so straightforward to demonstrate that it is indeed behaving quantum mechanically. For example, one could think of measuring the response $\langle\Phi(t)\rangle$ or $\langle Q(t)\rangle$ to a sinusoidal perturbation. However, because the harmonic oscillator is always in the correspondence limit for all quantum numbers, such measurements would not distinguish between classical and quantum behavior. Measurements of the fluctuations $\langle\Phi^2\rangle$ or $\langle Q^2\rangle$ would clearly distinguish quantum and classical behavior, but such measurements would require a quantum-limited amplifier at microwave frequencies.

For these reasons, the experiments reported in this paper involved a nonlinear inductor, namely a Josephson tunnel junction.[2] The macroscopic degree of freedom is the phase difference δ across the junction, a variable that is analogous to the flux Φ of the LC oscillator. The anharmonicity of the oscillator containing a Josephson junction has two important consequences. First, one can demonstrate the existence of a wave packet associated with δ by observing the decay of the metastable ground state by tunneling, a process that has become known as macroscopic quantum tunneling (MQT). Second, since the quantum and classical responses to an external sinusoidal perturbation are now different, one can demonstrate the existence of quantized energy levels spectroscopically. As emphasized by Leggett,[1] the use of an anharmonic oscillator enables one "to evade the correspondence limit."

The first theoretical description of MQT in Josephson junctions appears to be that of Ivanchenko and Zilberman.[3] A major step forward in the theory was made by Caldeira and Leggett[4] who discussed the reduction in the tunneling rate by the addition of a linear resistance that damped the junction. Subsequently, there have been many papers on the theory of MQT: An extensive list appears in Ref. 5. On the other hand, there have been relatively few experiments. Experiments on MQT in a Josephson junction were first carried out by Voss and Webb[6] and Jackel *et al.*[7] with closely related experiments on a junction in a superconducting loop by de Bruyn Ouboter and co-workers,[8] Prance *et al.*,[9] and Dmitrenko *et al.*[10] The results of most of these experiments were in qualitative agreement with theory in that the distribution of switching events as a function of bias current tended to flatten out when the temperature was lowered sufficiently. More recently there have been experiments[11,12] to test the temperature dependence of the effect of damping on the tunneling rate; the results were also qualitatively in accord with predictions. However, a persistent experimental difficulty has been a lack of knowledge of the junction parameters in the microwave frequency range relevant to the tunneling phenomenon. In particular, a crucial parameter is the complex impedance presented to the junction at microwave frequencies by the wires directly connected to it or by any circuit in its vicinity. In this context, we note that Schwartz *et al.*[11] carefully designed their experiment on an overdamped junction to minimize errors originating in the lack of knowledge of the behavior of the junction in the microwave range. Despite these efforts, the measured escape rates were in marked disagreement with theory,[13] although the predicted temperature dependence of the tunneling exponent was observed. The reasons for the discrepancy are still the subject of debate.[14]

The major difference between the present work and those experiments mentioned above is our use of *classical* phenomena to measure all the relevant parameters of the junction *in situ*, so that we are able to compare our experimental results with theory with no fitted parameters. We begin in Sec. II with a brief review of the resistively shunted Josephson junction and of the relevant predictions for macroscopic quantum tunneling. Section III is a description of our experimental techniques, while Sec. IV describes the measurement of the junction parameters. Sections V and VI contain our results for MQT and quantized energy levels. Section VI is a concluding discussion. Parts of this work has been reported elsewhere.[15–18]

II. THE CURRENT-BIASED JOSEPHSON TUNNEL JUNCTION AND THE ESCAPE FROM THE ZERO-VOLTAGE STATE

A. The current-biased junction

In our experiment we cool a Josephson tunnel junction to millikelvin temperatures and monitor its low-frequency electrical characteristics by means of room-temperature electronics. To isolate the junction from noise generated at room temperature, a series of cooled low-pass filters is inserted into the line connected to the junction [Fig. 1(a)]. The critical current of the junction is I_0, its self-capacitance is C_j, and its quasiparticle tunneling resistance is $R_{qp}(V)$, where V is the voltage across the junction. The loading of the junction by the filters can be represented by an admittance $Y_f(\omega)$ in parallel with the junction [Fig. 1(b)], where $\omega/2\pi$ is the frequency. The filter connected to the mount has been designed so that to a good approximation $Y_f(\omega)$ may be represented by a capacitance C_f in parallel with a resistance R_f over the relevant frequency range. This model, which has been ex-

tensively tested as we will describe in Sec. IV, is shown in Fig. 1(c). At the low temperatures of our experiment, the quasiparticle conductance is negligible and $R=R_f$. The capacitance $C=C_j+C_f$ is large enough for capacitance renormalization[19] arising from quasiparticle tunneling to be negligible. Note that in our experiment $C_j \gg C_f$. With these simplifications one regains the resistively shunted junction for which the equation of motion is

$$C\left[\frac{\Phi_0}{2\pi}\right]^2\ddot{\delta}+\frac{1}{R}\left[\frac{\Phi_0}{2\pi}\right]^2\dot{\delta}+\frac{\partial}{\partial\delta}\left[-\frac{I_0\Phi_0}{2\pi}\cos\delta-\frac{I\Phi_0}{2\pi}\delta\right]-\frac{\Phi_0}{2\pi}I_N(t)=0\ , \tag{2.1}$$

where δ is the difference in the phases of the order parameters on the two sides of the junction and $I_N(t)$ is the noise current generated by R. The dot implies differentiation with respect to time.

Equation (2.1) is also the equation of motion of particle of mass $C(\Phi_0/2\pi)^2$ moving in the one-dimensional (1D) potential

$$U(\delta)=-(I_0\Phi_0/2\pi)[\cos\delta+(I/I_0)\delta]\ .$$

This mechanical analog provides a useful insight into the dynamics of the junction. For $I \ll I_0$, the particle is in a stationary state in a particular well, and the voltage $V=\hbar\dot{\delta}/2e$ across the junction is zero. In the classical limit, if we neglect Nyquist noise for the moment, when I reaches I_0 the particle leaves the well and rolls down the washboard. In this regime $\dot{\delta}\neq 0$, and the voltage across the junction is nonzero. Provided the damping factor

$$\beta_c \equiv 2\pi I_0 R^2 C/\Phi_0 \gtrsim 1$$

the transition to the free-running state results in a sudden onset of voltage across the junction. When the current is subsequently reduced to zero, the junction reverts to the zero-voltage state.

Thus for $I<I_0$ the zero-voltage state is unstable. The height of the potential barrier is given by[20]

$$\Delta U=2U_0\{[1-(I/I_0)^2]^{1/2}-(I/I_0)\cos^{-1}(I/I_0)\}\quad (I<I_0) \tag{2.2}$$

$$\simeq(4\sqrt{2}U_0/3)(1-I/I_0)^{3/2},\quad [(I_0-I)/I_0 \ll 1]\ . \tag{2.3}$$

Here $U_0\equiv I_0\Phi_0/2\pi$. For the limit in which Eq. (2.3) is valid, ΔU is much less than the potential difference between adjacent wells, and, to a good approximation, the potential is cubic (Fig. 2). In the classical limit, the particle at the bottom of the well oscillates at a plasma frequency $\omega_p/2\pi$ where[20]

$$\omega_p=\omega_{p0}[1-(I/I_0)^2]^{1/4}\ , \tag{2.4}$$

and

$$\omega_{p0}=(2\pi I_0/\Phi_0 C)^{1/2}\ .$$

The damping factor is given by

$$Q=\omega_p RC\ . \tag{2.5}$$

In this paper we are concerned with the transition of the junction from the zero-voltage state for bias currents less than I_0. In the classical limit, the escape is induced by thermal noise that thermally activates the particle over the barrier. In thermal activation δ acts as a classical variable. In the quantum limit, on the other hand, the particle behaves as a wave packet and δ acts as a

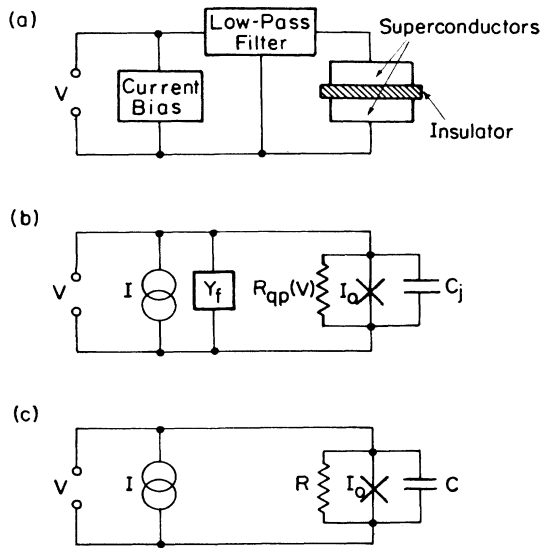

FIG. 1. (a) Current-biased Josephson junction with low-pass filter; (b) equivalent circuit of (a); (c) resistively shunted junction model obtained from the loading of the junction by a filter admittance consisting of a resistance and a capacitance.

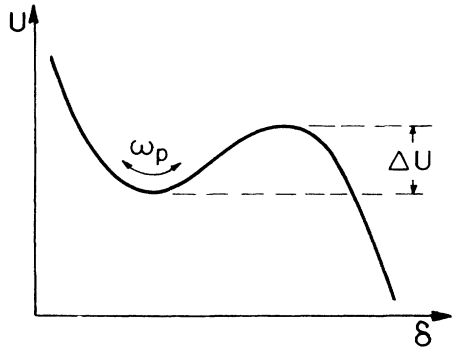

FIG. 2. Potential well from which particle escapes.

quantum-mechanical operator rather than as a c number. Since the tail of the wave packet extends under the barrier the particle can escape via MQT.

B. Predicted escape rates

The escape rate of a particle from a metastable state is a problem of long-standing importance. The current-biased Josephson junction is a simple example of this problem in which the metastable well is accurately modeled by a 1D cubic potential. The escape rate can be measured for values of $k_B T/\hbar\omega_p$ that range continuously from the classical limit ($k_B T/\hbar\omega_p \gg 1$) to the quantum limit ($k_B T/\hbar\omega_p \ll 1$). In this section we list the predicted escape rates for the low-damping limit ($Q \gg 1$) in which we are interested experimentally.

In the thermal regime, the escape of the particle from the well is driven by the Nyquist noise of the resistive shunt. In the moderate- to low-damping regime, the escape rate is given by[21]

$$\Gamma_t = a_t(\omega_p/2\pi)\exp(-\Delta U/k_B T) , \tag{2.6}$$

where, according to Büttiker *et al.*,[22]

$$a_t = 4\alpha/[(1+\alpha Q k_B T/1.8\Delta U)^{1/2}+1]^2 . \tag{2.7}$$

These authors found a best fit to numerical simulations with $\alpha = 1\pm 0.05$ although Risken and Voigtlaender[23] have proposed that the correct value of α is 1.4738. In this paper we require a knowledge of a_t only to make a small correction to the measured value of I_0, and we adopt the value $\alpha = 1$; nothing would be materially affected if instead one were to take the higher value of α.

In the quantum limit, if the macroscopic variable δ obeys quantum mechanics, the MQT rate at zero temperature in the absence of dissipation can be calculated in the Wentzel-Kramers-Brillouin (WKB) approximation. In the presence of a moderate level of dissipation, Caldeira and Leggett[4] have shown that for a cubic potential[24]

$$\Gamma_q = a_q \frac{\omega_p}{2\pi}\exp\left[-7.2\frac{\Delta U}{\hbar\omega_p}\left[1+\frac{0.87}{Q}+\cdots\right]\right] , \tag{2.8}$$

where

$$a_q \approx [120\pi(7.2\Delta U/\hbar\omega_p)]^{1/2} . \tag{2.9}$$

Equation (2.8) reduces to the WKB result in the limit $Q\to\infty$. The effect of dissipation is to localize the ground-state wave function (or, more strictly, density matrix) more strongly,[1] leading to an exponential dependence of the escape rate on the dissipation. Equation (2.8) is valid for the model junction shown in Fig. 2(c), where the resistance is ohmic. The more general case of an arbitrary admittance $Y(\omega)$ has been treated by several authors.[25–27]

We also need the prefactor in the intermediate-temperature range above the crossover temperature[28,29] $T_{cr} = \hbar\omega_p/2\pi k_B$ (in the weak-damping limit) that separates the thermal ($T \gg T_{cr}$) and quantum ($T \ll T_{cr}$) regimes. For $T \gtrsim 1.4T_{cr}$, the escape rate is[29]

$$\Gamma_i = a_i(\omega_p/2\pi)\exp(-\Delta U/k_B T) \tag{2.10}$$

where to first order in $1/Q$

$$a_i = \sinh(\hbar\omega_p/2k_B T)/\sin(\hbar\omega_p/2k_B T) . \tag{2.11}$$

At high temperatures Eq. (2.11) does not[30] reduce to Eq. (2.7), but since we use a_i only to make a small correction in I_0 (Sec. IV B), this discrepancy is unimportant.

In comparing experimentally determined escape rates with theoretical predictions, we will find it convenient to introduce the *escape temperature* T_{esc} which is defined through the relation

$$\Gamma = (\omega_p/2\pi)\exp(-\Delta U/k_B T_{esc}) . \tag{2.12}$$

In the thermal limit, comparing Eqs. (2.6) and (2.12) we find

$$T_{esc} = T/(1-p_t) \quad (k_B T \gg \hbar\omega_p) , \tag{2.13}$$

where

$$p_t = (\ln a_t)/(\Delta U/k_B T) . \tag{2.14}$$

Since a_t is close to unity $|p_t| \ll 1$. Thus in the thermal limit T_{esc} should be nearly equal to T. In the quantum limit at $T=0$, on the other hand, from Eqs. (2.8) and (2.12) we find

$$T_{esc} = \frac{\hbar\omega_p}{7.2k_B}\frac{1}{1+0.87/Q}\frac{1}{1-p_q} \quad (T=0) , \tag{2.15}$$

where

$$p_q = (\ln a_q)/[(7.2\Delta U/\hbar\omega_p)(1+0.87/Q)] . \tag{2.16}$$

The value of a_q is large enough to make the contribution from p_q substantial.

We use the escape temperature rather than the escape rate to express our results because in both the classical and quantum regimes T_{esc} is very nearly independent of the bias current. Thus the value of T_{esc} is a physically meaningful measure of the escape phenomenon with the dependence of circumstantial parameters such as the barrier height almost completely scaled out.

III. EXPERIMENTAL APPARATUS AND PROCEDURES

A. Design philosophy

We begin by discussing our choice of parameters for the tunnel junction. First, to satisfy the condition $\omega_0 \gtrsim 10k_B T/\hbar$ at the lowest temperature of our refrigerator, about 20 mK, we require $\omega_p(I)/2\pi \gtrsim 4$ GHz. On the other hand, to facilitate the necessary microwave engineering one should restrict the frequency to below 10 GHz. A reasonable compromise is $\omega_p(I)/2\pi \approx 5$ GHz. Second, if we assume that the measured circuitry attached to the junction has an impedance of roughly 50 Ω around the plasma frequency, to ensure a junction Q of at least 10 we require $1/\omega_p(I)C \lesssim 5$ Ω. These two conditions imply a minimum value for C of 6 pF. Third, to obtain escape rates sufficiently low to be measured accurately and sufficiently high to yield good statistical precision, we have to confine ourselves to a range in which $\Delta U(I)/\hbar\omega_p(I) \approx 2$ [from Eq. (2.8)]. Finally, to avoid having to achieve an unrealistically precise measurement of the value of bias current at which escape occurs the first

three criteria should be satisfied with $I/I_0 \lesssim 0.99$. These conditions lead us to choose $I_0 \approx 10\ \mu$A.

It is important to minimize the reactive loading of the junction by the circuitry to which it is attached. We assume that these stray reactances can be represented by a shunt capacitance C_f at high frequencies and a series inductance L_l at low frequencies that arises from the leads attached to the junction. Writing Eq. (2.8) in the form $\Gamma_q \propto e^{-B}$, one can show[26] that the changes ΔB in the exponent can be written in the form $\Delta B/B = 1 + C_f/2C_j$ and $\Delta B/B = 1 + 5L_J/2L_l$, where $L_J = 1/\omega_p^2 C$. Thus one should attempt to design the bias circuitry so that $C_f/C_j \ll 1$ and $L_J/L_l = 1/\omega_p^2 C L_l \ll 1$. For the parameters given above, these constraints imply $C_f \ll 6$ pF and $L_l \gg 0.15$ nH. In our experiment, we estimate that $C_f \lesssim 1$ pF while the inductance of the thin-film leads to our junction $L_l \gtrsim 5$ nH. Thus both constraints were reasonably well satisfied.

B. Equipment

We fabricated the junctions using standard photolithographic procedures on an oxidized silicon wafer that was subsequently diced to produce $10 \times 10\text{-mm}^2$ chips. The Nb base electrode, approximately 10 μm wide and 200 nm thick, was oxidized in a radio frequency discharge in an Ar-O_2 mixture, and a 300-nm-thick Pb (5 wt. % In) counterelectrode was deposited immediately afterwards. Two Nb pads and a single Pb-In pad were used to connect the junction to the mount (see below) via indium pellets. The I-V characteristics revealed high-quality junctions with low leakage. The ratio w/λ_J, where w is the width of the junction and λ_J is the Josephson penetration depth, was typically 0.05, so that the junction was comfortably in the "small-junction" limit.

The apparatus used to determine the lifetime of the zero-voltage state is shown in Fig. 3. A voltage ramp in series with a resistor generated a current through the junction. When the junction switched from the zero-voltage state, the resulting voltage was amplified (with a PAR 113 preamplifier, which has a very low-current noise) and used to gate a sample-and-hold circuit that captured the voltage across the resistor (0.3 to 2 MΩ). This measure of the current was digitized and transmitted to a computer outside the screened room surrounding the dilution refrigerator via an optical fiber link. A constant offset current was introduced so that we needed to digitize only a narrow range of current. The reproducibility of the current measurement was 2 parts in 10^5. After the junction had switched to the dissipative state, the current was turned off after an interval that could be varied. The power to the electronics was supplied by batteries, and careful tests were made to ensure that no digital noise was coupled into the junction.

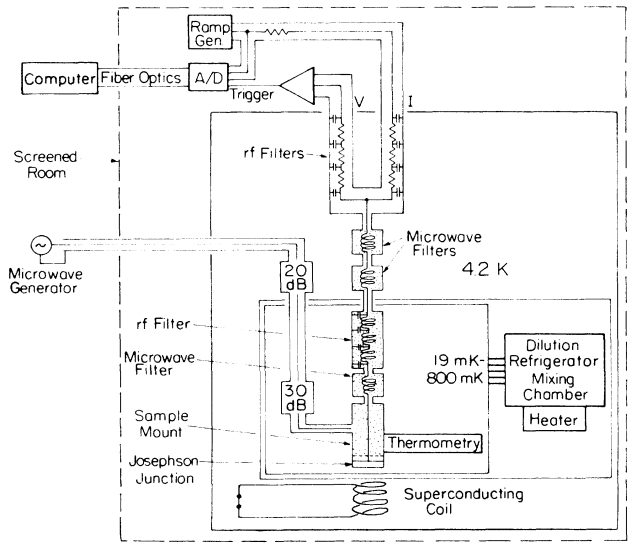

FIG. 3. Schematic drawing of apparatus.

We found it essential to use a chain of low-pass filters to exclude high-frequency noise from the junction. The current and voltage leads each contained a RC network at 4.2 K with a cutoff frequency of about 1 MHz. From 20–200 MHz the measured attenuation exceeded 60 dB. However, at higher frequencies the attenuation decreased appreciably, presumably because of stray capacitance across the resistors. For this reason, we developed a novel type of microwave filter consisting of a spiral coil of insulated Manganin wire inside a copper tube filled with copper powder with a grain size of about 30 μm. Since each grain appears to be insulated from its neighbors by a naturally grown oxide layer, the effective surface area is enormous, and the skin-effect damping produces a substantial attenuation. The measured attenuation of such a filter 0.1 m long was greater than 50 dB from 0.5–12 GHz. Two of these filters were installed in series at 4.2 K. The filters at 4.2 K eliminated room-temperature Nyquist noise and spurious rf and microwave radiation. A microwave and a rf filter were also required at the temperature of the junction to eliminate the Nyquist noise from the 4.2-K filters. In the case of the microwave filter, after filling the tube with the copper powder we injected Stycast 2850 epoxy to ensure good thermal contact. The 3-pole rf LC filter, also potted in copper powder and Stycast, provided an attenuation of more than 40 dB from 15–200 MHz. For the combined system of filters the attenuation exceeded 200 dB from 100 MHz to 12 GHz. It is noteworthy that we could connect to the bias leads the maximum output of a microwave generator tuned to the plasma frequency with no discernible effect on the escape rate. Thus we are confident that we had successfully eliminated spurious noise sources in this frequency range.

The mount (see Fig. 4) to which the junction was attached is an important component of the experiment. As the last filtering stage on the leads connected to the junction, the mount was responsible for all the resistive loading on the junction (we recall here that damping due to the quasiparticles is negligible). The mount was designed as an attenuating coaxial line to obtain a response as independent of frequency as possible. The attenuation, which was about 10 dB, was provided by the copper powder as in the other microwave filters. The separation of the junction from the end of the line was about 8 mm, less that a quarter wavelength at the plasma frequency.

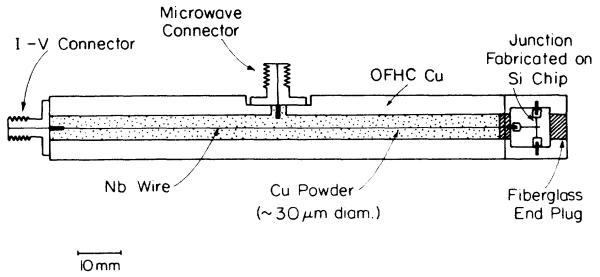

FIG. 4. Scale drawing of filter on which junction was mounted.

To avoid Joule heating from the bias current we used an insulated niobium wire as the central conductor. The thermal time constant of the mount, which we determined by using the escape rate of a junction in the classical regime to measure the temperature of the dissipative element, was less than 3 min at 20 mK (see Sec. V). The sub-minature series A (SMA) connector coupled microwave power capacitively into the junction with about 60 dB of attenuation. This coupling mode ensured that the junction was fed from a current source.

A magnetic field could be applied parallel to the plane of the junction by means of a superconducting solenoid, operated in the persistent current mode, wound on a copper end cap that was clamped over the lower end of the mount. A thermal switch mounted on the 1-K pot enabled us to charge the solenoid by means of a second superconducting solenoid wound on the vacuum can of the refrigerator. Two μ-metal shields around the liquid-^{4}He Dewar were used to reduce the ambient magnetic field.

Three thermometers were attached to the mount. A calibrated Ge resistance thermometer, calibrated in a separate experiment, was used at temperatures above 100 mK with an estimated accuracy of ± 2 mK. From 19 mK to about 35 mK, a ^{60}Co nuclear orientation thermometer was used, with an estimated accuracy that varied from ± 2 mK at 20 mK to ± 4 mK at 35 mK. A Speer carbon resistance thermometer was calibrated in these two temperature ranges and an interpolation used between 35 and 100 mK to give an estimated accuracy of ± 5 mK. The temperature could be raised by means of a heater attached to the mixing chamber.

C. Determination of escape rate

In our determination of the escape rate we collected 10^4 to 10^5 events for each set of parameters, the digitized value of the bias current at which each event occurred being stored in a computer. The resulting distribution of the switching probability $P(I)$ was used to compute the mean escape rate out of the zero-voltage state[20] as a function of I:

$$\Gamma(I)=\frac{1}{\Delta I}\frac{dI}{dt}\ln\left[\sum_{i\geq I}P(i)\Big/\sum_{i\geq I+\Delta I}P(i)\right]. \tag{3.1}$$

Here, dI/dt is the current ramp rate and ΔI is the channel width of the analog-to-digital converter. Typically, we measured escape rates in the range 10^2 to 10^6 s^{-1}; this range corresponds to a relatively small variation in the value of I. Note that as the escape temperature changes, for fixed values of ΔI and dI/dt, the range of I in which a given range of Γ occurs also changes.

A very important consideration is the Joule heating of the junction after it has switched out of the zero-voltage state. Although the dissipation ceases when the junction is reset to zero voltage, one must ensure that the junction cools down to the equilibrium temperature before the next escape event occurs. Two times are important in this return to equilibrium, the thermal time constant $\tau_{\rm cool}$ for the junction to cool, and the time $\tau_{\rm zero}$ (which is longer than Γ^{-1}) that the junction spends in the zero-voltage state. If $\tau_{\rm cool}<\tau_{\rm zero}$, one can vary $\tau_{\rm zero}$ (by varying the time that elapses before starting the current ramp) to determine whether the measured value of Γ depends on $\tau_{\rm zero}$. If $\tau_{\rm cool}>\tau_{\rm zero}$, on the other hand, the temperature of the junction is not very dependent on $\tau_{\rm zero}$, but increases with the power dissipated in the voltage state. One can vary this power by varying the duty cycle, that is, the percentage of a ramp cycle that the junction spends in the dissipative state. At constant duty cycle, when we varied the repetition rate from 20 to 4 s^{-1} (thereby varying $\tau_{\rm zero}$) the value of $T_{\rm esc}$ did not change for a junction in the classical regime at 18 mK. However, we found that $T_{\rm esc}$ increased by 10% when we increased the duty cycle from 1% to 20%, but when we decreased the duty cycle from 1% to 0.1% the change in $T_{\rm esc}$ was imperceptible. We obtained all our measurements with a duty cycle of 0.1% to preclude heating effects.

We note in passing that since dissipation at the plasma frequency is entirely dominated by losses in the mount, the temperature "seen" by the junction is that of the mount rather than that of the junction itself. Thus the temperature of the junction could in fact be raised significantly above the equilibrium value without changing the escape rate.

IV. DETERMINATION OF JUNCTION PARAMETERS BY CLASSICAL METHODS

We now describe a series of measurements made on a single junction at about 15 temperatures between 18 and 800 mK to obtain C, R, and I_0 with purely classical phenomena. The measurements were made for three values of I_0, the low and middle values being obtained near the first minimum and first maximum, respectively, of the diffraction patternlike response to an applied magnetic field. Each value of I_0 gave access to a particular range of plasma frequency, which scaled as $I_0^{1/2}$ for a given value of I/I_0. Once we had established a particular value of I_0, we obtained data over the entire temperature range (including the quantum regime) before resetting I_0.

A. Resonant activation

We have given a detailed account of resonant activation elsewhere[15,31]; several other theoretical papers on the subject have also appeared.[32–34] For the present purpose, it is sufficient to know that when a microwave current is ap-

plied to a current-biased junction in its zero-voltage state, there is an enhancement of the escape rate from this state. As the microwave frequency is varied the enhancement goes through a pronounced maximum in the vicinity of the plasma frequency. Observation of the resonance offers a new way to determine ω_p and Q. At each temperature we determine the escape rates $\Gamma(0)$ in the absence of microwaves and $\Gamma(P)$ in the presence of microwave power[35] P. The power level was adjusted to obtain $\ln\gamma = \ln[\Gamma(P)/\Gamma(0)] < 1$, the range over which $\ln\gamma$ is linear[31] in P. We kept the microwave frequency $\Omega/2\pi$ constant and varied $\omega_p(I)$ by measuring the change in escape rates over the range of bias current that produced measurable values of Γ. The used of a fixed microwave frequency eliminates difficulties associated with frequency-dependent coupling between the generator and the junction. Figure 5(a) shows an example of the variation of $\ln\gamma$ with I. The scatter in the data at high and low currents arises from the relatively small number of switching events recorded in the regions. Since the current range is small compared with $I_0 - I$, the plasma frequency is nearly linear in I. Plots similar to this were obtained at one to three microwave frequencies at each of a number of values of temperature so that the plasma frequency could be obtained over a wide range of current.

We emphasize that the observed resonant behavior is an intrinsic property of the junction. It cannot arise from parasitic resonances that may exist in the microwave injection circuit. In these measurements the microwave frequency is *fixed*, and one sweeps the plasma frequency through it by varying the bias current. Thus, the injected microwave power is kept constant. Parasitic resonances in the mount could affect the junction, but these resonances would not depend on I or I_0. We show in this paper and in a separate series of experiments[15,31] that the position of the resonances varies correctly with I_0. Lastly, the observed classical resonances are highly asymmetric as predicted for the nonlinear inductance of the junction.

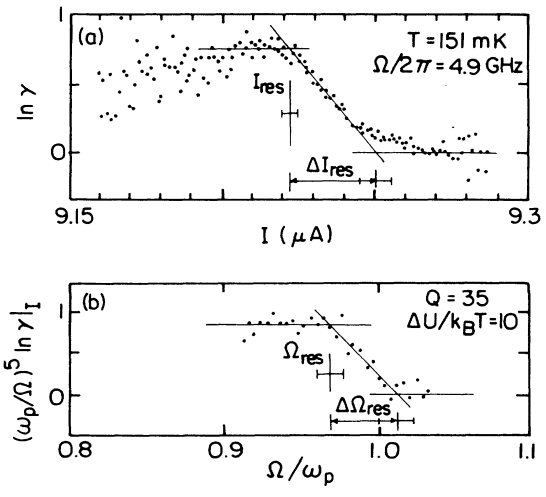

FIG. 5. (a) Experimentally determined values of $\ln\gamma$ vs I (solid circles), with estimates of $I_{\rm res}$ and $\Delta I_{\rm res}$ indicated. (b) Simulated resonant activation data showing constructions for $\Omega_{\rm res}$ and $\Delta\Omega_{\rm res}$ and their estimated uncertainties.

To interpret our data we have carried out a series of numerical simulations in which we computed $\ln\gamma$ versus Ω for known values of ω_p and Q. Since in the experiments Ω was fixed while ω_p and ΔU were varied, one must scale $\omega_p(I)$ and $\Delta U(I)$ in the simulations to compare the results with the experimental data. We show elsewhere[31] that in the linear regime for fixed I

$$\ln\gamma(\Omega)\,|_I \propto (P\Delta U/\omega_p T^2) f(\Omega/\omega_p, Q) \ , \tag{4.1}$$

where $f(\Omega/\omega_p, Q)$ is a resonant function known from numerical simulations. Since, from Eqs. (2.3) and (2.4), $\Delta U \propto (1 - I/I_0)^{3/2}$ and $\omega_p \propto (1 - I/I_0)^{1/4}$, for fixed microwave frequency we have

$$\ln\gamma(I)\,|_\Omega \propto (\omega_p/\Omega)^5 \ln\gamma(\Omega)\,|_I \ . \tag{4.2}$$

In Fig. 5(b) we have plotted $(\omega_p/\Omega)^5 \ln\gamma(\Omega)\,|_I$ obtained from simulations versus Ω/ω_p. The experimental and simulated data have similar shapes; this was always true provided $k_B T/\hbar\Omega > 0.6$.

The essential features of the resonances are the position and width, which we define using the following procedures [see Fig. 5(b)]. We draw a horizontal line through the maximum of the simulated data, and a second line through the region of maximum negative slope. The intersection of these two lines defines the reduced resonant frequency $\Omega_{\rm res}/\omega_p$, while the separation of this frequency from the intersection of the slanted line with $\ln\gamma = 0$ is the reduced resonance width $\Delta\Omega_{\rm res}/\omega_p$. In Table I we list $\Omega_{\rm res}/\omega_p$ and $\Delta\Omega_{\rm res}/(\omega_p/Q)$ for four values of Q. For the purpose of the ensuing measurements we adopt the average value

$$\Omega_{\rm res} = 0.96\omega_p \ . \tag{4.3}$$

In the case of the width of the resonance, since our main object is to establish a *lower* bound on Q we have taken the conservative estimate

$$\Delta\Omega_{\rm res} = \omega_p/Q \ . \tag{4.4}$$

We used the same constructions to obtain $I_{\rm res}$ and $\Delta I_{\rm res}$ from the experimental data, as shown in Fig. 5(a). Equa-

TABLE I. Values of $\Omega_{\rm res}/\omega_p$ and $\Delta\Omega_{\rm res}/(\omega_p/Q)$ obtained from numerical simulation of resonant activation.

Q	$\Omega_{\rm res}/\omega_p$	$\Delta\Omega_{\rm res}/(\omega_p/Q)$
10	0.958±0.012	1.00±0.30
15	0.960±0.012	1.15±0.30
25	0.962±0.010	1.31±0.40
35	0.968±0.008	1.52±0.40

tion (4.3) implies

$$\omega_p(I)=\Omega/0.96 \quad \text{at } I=I_{\rm res} \ . \tag{4.5}$$

In Fig. 6 we plot $I_{\rm res}$ versus $[(\Omega/2\pi)/0.96]^4$ for the high value of critical current for many resonant activation measurements with $k_BT/\hbar\omega>0.6$; the error bar for each point arises from the uncertainty in the determination of $I_{\rm res}$. Using Eq. (2.4) we have drawn a curve through the data using the values of I_0 and C indicated (the way in which these values were chosen will be discussed later). This procedure yields a first approximation to the values of I_0 and C.

Having established $\omega_p(I)$ and I_0, we next determine Q using Eq. (4.4) with $\Delta\Omega_{\rm res}=\Delta I_{\rm res}\partial\omega_p/\partial I$. We find

$$Q=\{2[1-(I/I_0)^2]/(I/I_0)\}I_0/\Delta I_{\rm res} \ . \tag{4.6}$$

In Fig. 7 we plot the values of Q, obtained from resonant activation at the three values of I_0 versus $\omega_p/2\pi$. The errors arise from the uncertainties in extracting Q from the data. We note that Q exhibits a considerable amount of structure, and that its trend fails to exhibit the expected proportionality to ω_p. These features emphasize the complicated nature of the admittance presented to the junction. We have thus approximated Q by the frequency-independent value of $Q=30\pm15$.

A more sophisticated analysis[31] of the phenomenon of resonant activation yields values of ω_p and Q that are very close to the values found by the methods described here.

B. Determination of I_0

Now that we have $\omega_p(I)$, we are in a position to determine I_0 from the exponential dependence of Γ on I in the thermal regime without microwaves. As is evident from

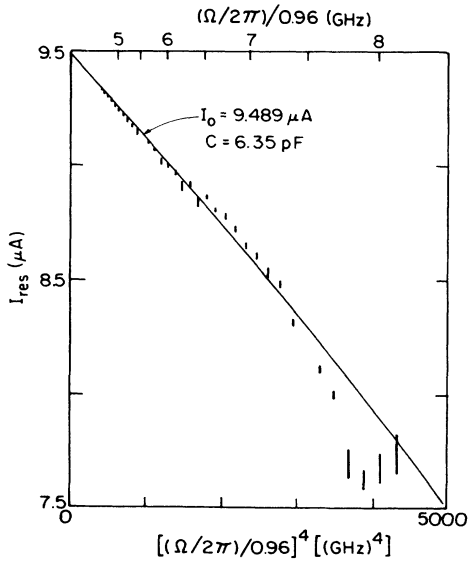

FIG. 6. $I_{\rm res}$ vs $[(\Omega/2\pi)/0.96]^4$ obtained from resonant activation data at several temperatures. Error bars represent uncertainty in $I_{\rm res}$. The curve is the prediction of Eq. (2.4) with $I_0=9.489$ μA and $C=6.35$ pF.

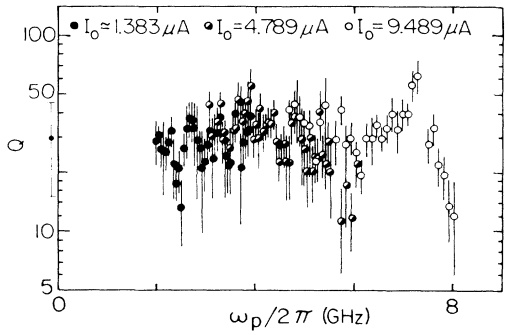

FIG. 7. Q vs $\omega_p/2\pi$ for three values of I_0. The average value of 30 ± 15 is shown to the left of the figure.

the expression for Γ_t and ΔU [Eqs. (2.3) and (2.6)], a plot of the experimentally determined quantity $\{\ln[\omega_p(I)/2\pi\Gamma(I)]\}^{2/3}$ versus I should yield a straight line with slope scaling as $T_{\rm esc}^{-2/3}$ that intersects the current axis at I_0. We neglect for the moment possible corrections due to the fact that a_t is not exactly unity and that we have used the cubic approximation for ΔU. Figure 8 shows five examples of such plots for the high value of I_0. A least-squares fit, weighted according to the square root of the number of escape events included in each point, was used to draw lines through the data at the three highest temperatures. Each line intercepts the current axis at I_0(intercept), the values of which are very nearly independent of temperature. Figure 8 also shows data taken at 46 and 19 mK. The slope is almost identical at these two temperatures, indicating that $T_{\rm esc}$ changes very little as the temperature is lowered from 46 to 19 mK.

Figure 9(a) shows the values of I_0(intercept) obtained from plots such as those in Fig. 8. The uncertainty represents ±1 standard deviation in the least-squares analysis. We observe that I_0(intercept) decreases by about 0.05% as the temperature is lowered from 800 to 50 mK. However, we have to make small corrections to I_0(intercept) to obtain the true value of I_0.

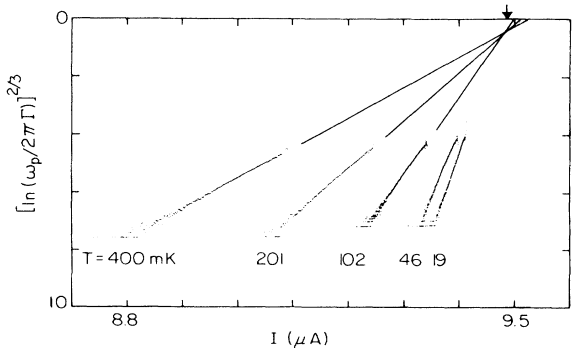

FIG. 8. $\{\ln[\omega_p/2\pi\Gamma(I)]\}^{2/3}$ vs I for 5 temperatures. Least-square fits to the data at the three highest temperatures intersect the current axis at I_0 (intercept); the arrow indicates the value of I_0 after corrections to I_0 (intercept) have been made.

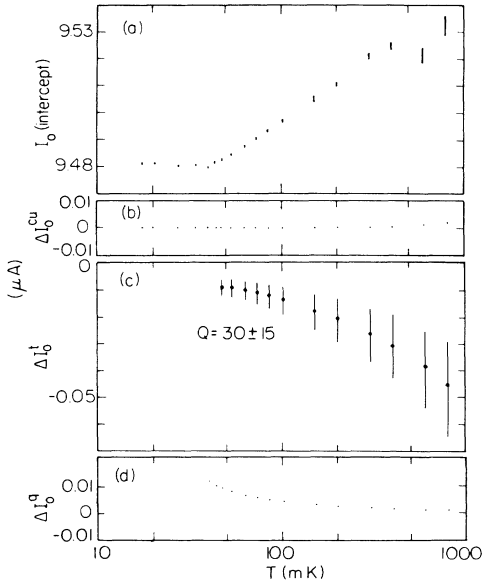

FIG. 9. (a) I_0(intercept) vs T for high value of I_0. Corrections for (b) cubic approximation ΔI_0^{cu} (c) thermal prefactor ΔI_0^t, and (d) quantum prefactor ΔI_0^q are also shown.

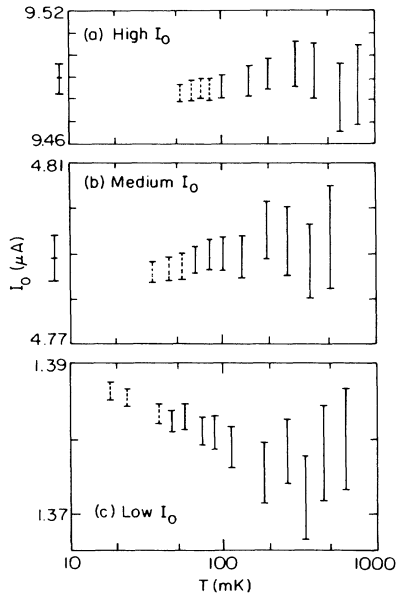

FIG. 10. Corrected values of I_0 vs T. Dashed lines are for $1.4T_{cr} < T < 3T_{cr}$ where quantum corrections are nonnegligible. In (a) and (b) the average value of I_0 including the dashed data is shown to the left of the current axis.

The correction in I_0 for the cubic approximation is

$$\Delta I_0^{cu} = I_0/\{s_m + 3[(1-s_m^2)^{1/2} - s_m \cos^{-1} s_m]/2\cos^{-1} s_m\} - I_0 ,$$

where s_m is the value of I/I_0 weighted most heavily in the least-squares fit for I_0(intercept). Figure 9(b) shows ΔI_0^{cu} versus T. The departure of the thermal prefactor a_t from unity produces the correction

$$\Delta I_0^t = I_0(1-s_m)[(\ln a_t)/B - (\partial a_t/\partial B)/a_t] ,$$

where $B = \Delta U/k_B T$, a_t is given by Eq. (2.7) and a_t, B and $\partial a_t/\partial B$ are evaluated at s_m. In Fig. 9(c) we plot ΔI_0^t versus T with $Q = 30 \pm 15$ for $T > 1.4T_{cr}$.

As mentioned in Sec. II, in the low-damping regime there is no exact expression for the quantum corrections to the prefactor of the thermal escape rate. As an approximation we obtain an estimate for the quantum correction by using Eq. (2.11) in the expression for ΔI_0^t, with a_t replaced by a_i. The correction ΔI_0^q is plotted versus T in Fig. 9(d), and is small above $T = 3T_{cr} \approx 90$ mK.

Figure 10 shows all three corrected values of I_0 versus T for $T > 1.4T_{cr}$. Data in the range $1.4T_{cr} < T < 3T_{cr}$ are shown dashed to indicate that the prefactor correction is somewhat uncertain. To within the experimental uncertainty, I_0 is independent of temperature in Figs. 10(a) and 10(b). On the other hand, in Fig. 10(c) we observe a slight temperature dependence, possibly because I_0 was strongly dependent on the applied magnetic field, the value of which could have changed slightly with temperature. Since these data are used only to check the escape rate in the thermal limit, this small temperature dependence is not a serious problem: Below 100 mK we used the temperature-dependent values with an error of ± 0.005 μA.

We should like to emphasize several features of this method of determining I_0. First, the value of T_{esc} is an independent measure of the temperature of the dissipative element, so that our estimate of I_0 does not involve a knowledge of the temperature. Second, the lack of curvature in plots such as those in Fig. 8 gives some evidence that spurious low-frequency noise, which would distort the distribution of switching events, was negligible. Third, the temperature independence of I_0 in Figs. 10(a) and 10(b) lends some experimental support for the classical prefactor, the correction for which dominates the other two corrections. Finally, this constancy of I_0 with temperature provides good reason to believe that it did not change with temperature below 50 mK.

C. Values of C and R

The value of I_0 obtained from the temperature dependence of $\Gamma(I)$ is considerably more accurate than the value obtained from resonant activation. We use this new value of I_0 with $\omega_p(I)$ to obtain a revised value of C that in practice does not differ significantly from the original estimate. A plot of C versus $\omega_p/2\pi$ obtained in this way is shown in Fig. 11(a), where data are shown for all three values of I_0; the error bars arise from the uncertainty in the determination of the value of ω_p from the resonant activation curves. The systematic error ΔC in C due to the uncertainty in I_0 is shown in Fig. 11(b).

There are several noteworthy features in Fig. 11(a). The values of C obtained at the same plasma frequency but at different values of I_0, and hence at different bias currents and temperatures, are in good agreement. For example, the 4.8-GHz points for the high and middle values of I_0 were taken at 100 and 600 mK, respectively. This agreement supports the expectation that C is in-

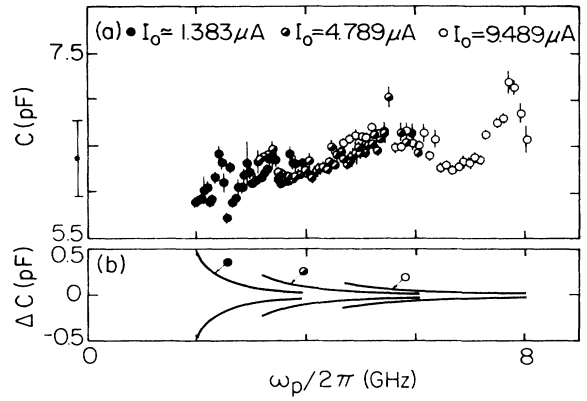

FIG. 11. (a) C vs $\omega_p/2\pi$ for three values of I_0; (b) systematic error ΔC in C due to the uncertainty in I_0.

dependent of I_0, I, and T. On the other hand, C varies somewhat with the plasma frequency, presumably because of the complicated admittance presented to the junction by the leads and the mount. It is only because we deliberately choose a rather large junction capacitance that this spurious reactance did not pose serious problems. We have represented the capacitance by the single value 6.35±0.4 pF shown to the left of Fig. 11(a). We believe that any systematic error due to the approximation of the frequency-dependent value of C by one frequency-independent value is included in this uncertainty. This value of C and the value of I_0 obtained from Fig. 10(a) have been used to draw the curve in Fig. 6.

As a check on our procedures the values of I_0 and C were iterated once more to ensure that they were consistent. This iteration is strongly convergent because the determination of I_0 from the current dependence of $\Gamma(I)$ depends only logarithmically on ω_p and Q. For example, a change in C of 0.4 pF and in I_0 of 0.007 μA changes the high value of I_0 by only 0.0003 and 0.0002 μA, respectively.

The values of $R(\omega_p)$ deduced from the values of Q and C are plotted in Fig. 12. We see that as ω_p increases R varies rapidly with a generally decreasing trend. At the plasma frequency of about 4 GHz that was used in the

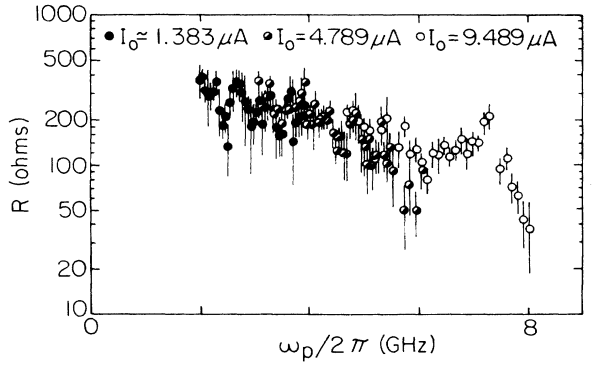

FIG. 12. R vs $\omega_p/2\pi$ obtained from Fig. 7.

MQT experiments for the high value of I_0 the value of R is 190±100 Ω. This value is very much less than the quasiparticle resistance of the junction at low voltages (>2 kΩ), and demonstrates that the dissipation is completely determined by the circuitry connected to the junction. Fortunately, for the present case of weak damping, the effect of Q on the MQT rate is small and the large variations in R do not lead to large errors in the prediction of T_{esc}. It is clear that the resistively shunted junction model is only an approximation to the real system.

V. DETERMINATION OF T_{esc}

Using the measured values of I_0, C, and R we computed T_{esc} from our data as a function of I and T using Eq. (2.12). In Fig. 13 we plot T_{esc} versus T for the high value of I_0 (solid circles) for $\ln(\omega_p/2\pi\Gamma)=11$; since, as we shall see, T_{esc} is weakly dependent on I, it is necessary to fix the value of ω_p/Γ at which the data are presented. The predicted value of T_{cr}, 30 mK, is indicated with a solid arrow. At temperatures above 100 mK, the measured values of T_{esc} are very close to the temperature T, as we expect in the thermal regime. At temperatures below 25 mK, on the other hand, T_{esc} becomes independent of temperature, with a value of 37.4±4 mK. The Caldeira-Leggett prediction at $T=0$ is $T_{esc}=36.0\pm1.4$ mK, which is in very good agreement with the temperature-independent value observed in our experiment. These values are summarized in Table II. The contribution of the damping to the predicted value of T_{esc} is −1.5 mK, which is less than the combined uncertainty of the theoretical prediction and experiment. As a result, we cannot make any statement about the effect of dissipation on quantum tunneling. The agreement of the measured and predicted values of T_{esc} in the quantum limit corresponds to an agreement of better than a factor of 4 in the escape rates, with no adjustable parameters.

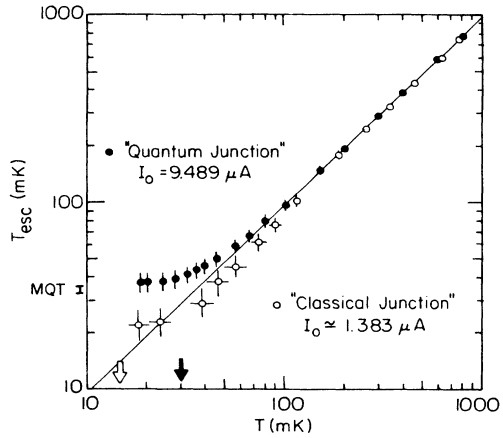

FIG. 13. T_{esc} vs T at $\ln(\omega_p/2\pi\Gamma)=11$ for the high and low values of I_0 with arrows indicating T_{cr} (solid and open circles and arrows). The prediction of Eq. (2.15) for $I_0=9.489$ μA is shown to the left of the T_{esc} axis. For clarity, error bars for T have been shown for the "classical junction" only; identical errors apply to the "quantum junction." The line is the thermal prediction $T_{esc}=0.95T$.

TABLE II. Junction parameters and T_{esc} for two values of I_0 at $\ln(\omega_p/2\pi\Gamma)=11$.

Admittance loading junction:
$C=6.35\pm0.4$ pF
$Q=30\pm15$
High value of I_0 ("quantum junction"):
$I_0=9.489\pm0.007$ μA
$T_{cr}=30$ mK
T_{esc} (extrapolated to $T=0$, measured)$=37.4\pm4.0$ mK
T_{esc} (predicted at $T=0$)$=36.0\pm1.4$ mK
Low value of I_0 ("classical junction"):
$I_0=1.386\pm0.005$ μA
$T_{cr}=15$ mK
T_{esc} ($T=19$ mK, measured)$=22\pm4$ mK
T_{esc} ($T=19$ mK, predicted)$=18\pm2$ mK

We note that the error in the measured values of T_{esc} is dominated by the uncertainty in ΔU, which arises, in turn, from the uncertainty in I_0. The error in the predicted value of T_{esc} in the quantum limit, on the other hand, arises largely from the uncertainties in ω_p (due to the error in C) and in Q. The error in the predicted value of T_{esc} in the classical limit is mostly due to the uncertainty in T.

Although the low-temperature values of T_{esc} are in good agreement with the $T=0$ prediction, nevertheless one should demonstrate that the flattening of T_{esc} as T is lowered is not due to an unknown, spurious noise source: In other words, we wish to show that the temperature "seen" by the junction is equal to the temperature indicated by our thermometers. For this reason, in Fig. 13 we have also plotted T_{esc} for the same junction with a reduced value of I_0 ("classical junction"), again for $\ln(\omega_p/2\pi\Gamma)=11$. The errors in our temperature scale have been indicated on these data: Identical error bars apply to the data for the "quantum junction," but have been omitted for clarity. Since $T_{cr}=15$ mK, we expect T_{esc} to be close to the classical prediction except, possibly, at the lowest temperature. To compare these values of T_{esc} with the classical prediction, we need to compute the departure of T_{esc} from T due to the departure of a_t from unity. For $Q=30$ and $\Delta U/k_BT=11$, Eq. (2.7) with $\alpha=1$ yields $a_t\approx0.60$. Thus from Eq. (2.14) we find $p_t\approx-0.047$ and from Eq. (2.13) the result $T_{esc}\approx0.95T$ plotted in Fig. 13. Above about 150 mK, both sets of data follow this prediction very closely. At lower temperatures, however, the data for the "classical junction" fall somewhat below the predicted values of T_{esc}. However, when one takes into account the errors in both T_{esc}, and T, one sees that this deviation is not significant. The point at the lowest temperature lies above the classical prediction, and probably heralds the onset of MQT. The important conclusion from these data is that their values of T_{esc} at low temperatures lie significantly below the values for the quantum junction, so that the flattening of the latter cannot arise from spurious noise sources.

There is, however, one other remote possible explanation for the flattening of T_{esc} for the quantum junction. Since the low-temperature measurements in the classical limit were made at a low critical current, and thus in a low range of bias current, we performed an additional experiment to ensure that the flattening of T_{esc} did not arise from Joule heating in the current line. Using the same mount and filters we made measurements on a 10×80 μm^2 junction with a critical current of about 30 μA for which $T_{cr}\approx20$ mK. At a temperature 24 mK, we measured $T_{esc}=23\pm3$ mK, implying that heating effects with a current as high as 30 μA were negligible.

Finally, we briefly discuss the effects of the prefactors a_t and a_q. An important difference between the thermal and quantum regimes can be observed through the weak dependence of T_{esc} on I, which arises from the different forms of a_t and a_q, and from the current dependence of ω_p. This behavior is illustrated in Fig. 14 for the high critical current junction. Figure 14(a) shows T_{esc} versus I in the thermal regime ($T=151$ mK) together with the prediction of Eq. (2.13). The predicted value of T_{esc} is less than T because $a_t<1$. Similarly, the fact that $a_t<1$ causes T_{esc} to decrease as the bias current is increased. Within the experimental uncertainties, the data agree well with the predictions. Figure 14(b) shows T_{esc} versus I in the quantum regime ($T=19$ mK), together with the prediction of Eq. (2.15). In this limit, T_{esc} increases with increasing bias current through the current dependence of ΔU because $a_q\gg1$; the current dependence of ω_p is relatively unimportant. Again, within the experimental uncertainties, the data are in good agreement with theory. We note that the error bars in Fig. 14 represent a systematic shift in each of the curves due to the uncertainties

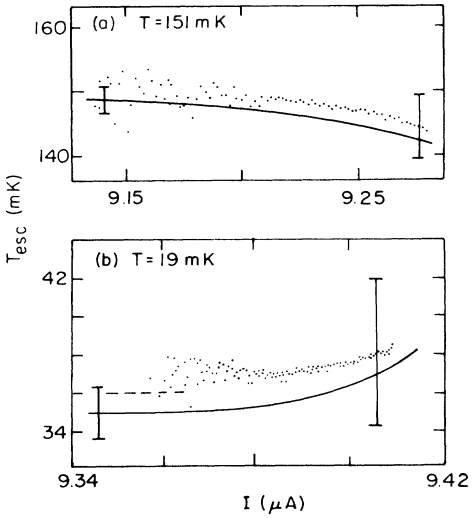

FIG. 14. T_{esc} vs I for $I_0=9.489$ μA in the (a) classical and (b) quantum regimes. Points are experimental data and solid lines are theoretical predictions. Dashed line in (b) is prediction for $Q\rightarrow\infty$. Error bars on left and right represents possible shift in the experimental and theoretical curves, respectively, due to uncertainties in the experimental parameters.

in the junction parameters. The very different current dependence of T_{esc} at high and low temperatures lends further support to the claim that the escape mechanisms are different in the two regimes.

In Fig. 15 we plot T_{esc} versus I at 10 temperatures that embrace the crossover temperature range. These data show the progressive transition from the classical to the quantum dependence of T_{esc} on the bias current as the temperature is lowered. We see that the current dependence of the escape rate changes qualitatively between 73 and 54 mK, that is, at a temperature of roughly $2T_{cr}$, where $T_{cr} \approx 30$ mK.

VI. QUANTIZED ENERGY LEVELS

A. Experiment

We now describe the effect of microwaves on the escape rate from the zero-voltage state when the junction is at or near the quantum limit. The purpose is to demonstrate spectroscopically the existence of quantized energy levels in the potential well. Since the effect of the microwaves is to induce transitions from one state to another of higher energy, and the escape rate out of the well increases when the population of states of higher energy increases, a resonant increase in the escape rate is expected when the microwave photon energy corresponds to an energy-level separation. As with the classical resonant activation measurements, we detected the resonances by varying the energy-level spacings with the bias current while keeping the microwave frequency fixed.

The energy in the well should be quantized as illustrated in Fig. 16(a). In Fig. 16(b) we plot the normalized spacings between adjacent energy levels $E_{n,n+1}/\hbar\omega_p$ versus $\Delta U/\hbar\omega_p$, the normalized potential height. We obtained the energy levels by solving the Schrödinger equation numerically using the boundary condition on the eigenfunctions $\psi_n(\delta)=0$ at the value of δ where the energy was equal to the potential energy on the free-running side of the barrier. This approximation leads to a negligible error in the eigenvalues because the probability of tunneling through the barrier is generally exceedingly small. In these and subsequent calculations of the energy levels we have neglected Lamb shifts due to the coupling of the junction to the resistor;[26] these shifts are negligible compared with the broadening of the levels. The anharmonicity of the cubic potential causes the spacing between adjacent levels to decrease with increasing energy in the well. As $\Delta U/\hbar\omega_p$ is increased, there are more metastable states in the well, and the spacing of the levels at the bottom of the well approaches that for the harmonic oscillator $\hbar\omega_p$.

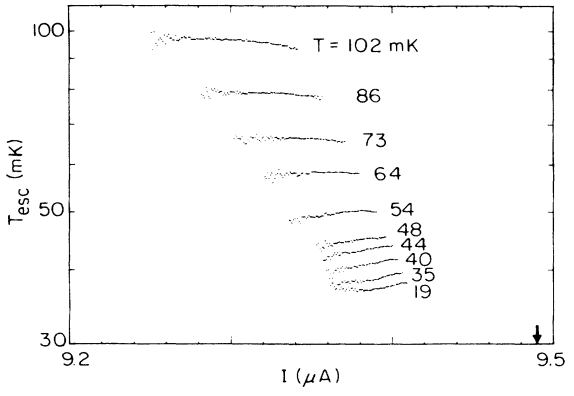

FIG. 15. T_{esc} vs I with $I_0=9.489$ μA (indicated by arrow) for $T \lesssim 102$ mK. For clarity data between 19 and 35 mK are not shown; data at 25 mK were indistinguishable from those at 19 mK.

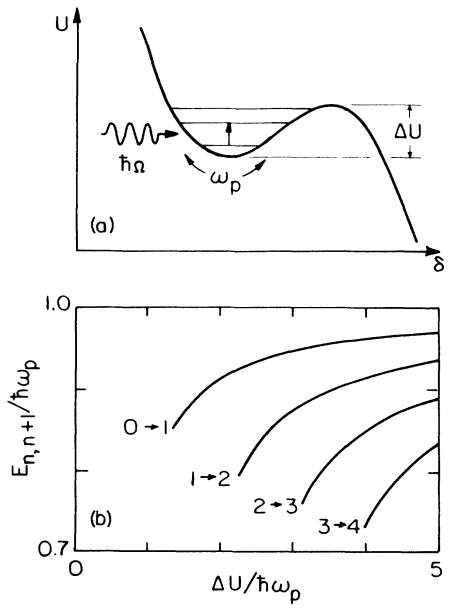

FIG. 16. (a) Cubic potential U vs δ showing three energy levels. Transition from the ground state to the first excited state induced by a photon of frequency $\Omega/2\pi$ is shown. (b) Difference in energy between the nth and the $(n+1)$th energy level $E_{n,n+1}/\hbar\omega_p$ vs potential height $\Delta U/\hbar\omega_p$ for $n=0,1,2,3$. Each curve terminates on the left when $E_{n+1}=\Delta U$.

The change in the escape rate was measured when a microwave current at fixed power P and frequency $\Omega/2\pi$ was injected into the current bias. The microwave power was chosen so that the enhancement $\gamma=\Gamma(P)/\Gamma(0)$ was linear in P. We note that in the quantum limit γ is linear in P for $\gamma(P) \lesssim 13$, in contrast with classical resonant activation where γ is linear[31] in P for $\gamma \leq 2$. Since the measurement of a change in the escape rate $[\Gamma(P)-\Gamma(0)]/\Gamma(0)$ is accessible over a range of bias currents, one can vary the bias current to sweep the energy-level spacings through the microwave frequency. Typical results appear in Figs. 17–20.

In Fig. 17(a) we show the change in escape rate due to 2.0-GHz microwaves for a junction with larger capacitance and critical current than that studied in Secs. IV and V. For the range of I shown in Fig. 17(a) the well contained several energy levels ($\Delta U/\hbar\omega_p \approx 6$), there was significant thermal population of the energy levels ($k_B T/\hbar\Omega \approx 0.3$), and the damping was sufficiently low to produce distinct resonances. Three peaks in $[\Gamma(P)-\Gamma(0)]/\Gamma(0)$ were observed, indicating that the es-

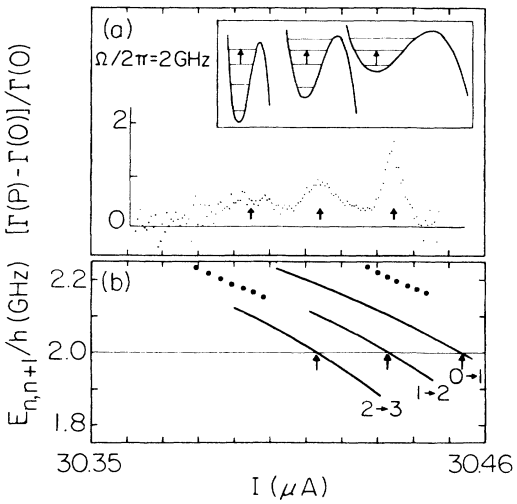

FIG. 17. (a) $[\Gamma(P)-\Gamma(0)]/\Gamma(0)$ vs I for a 80×10 μm^2 junction at 28 mK in the presence of 2.0 GHz microwaves ($k_BT/\hbar\Omega=0.29$). Arrows indicate positions of resonances. Inset represents the corresponding transitions between energy levels. (b) Calculated energy level spacings $E_{n,n+1}$ vs I for $I_0=30.572\pm0.017$ μA and $C=47.0\pm3.0$ pF. Dotted lines indicate uncertainties in the $0\rightarrow1$ curve due to uncertainties in I_0 and C. Arrows indicate values of bias current at which resonances are predicted.

cape is resonantly enhanced at certain values of the bias current. This is in striking contrast to the shapes of the resonances observed in classical resonant activation (Fig. 5). No further peaks were observed at higher values of bias current. These discrete resonances are characteristic of transitions between quantized energy levels.

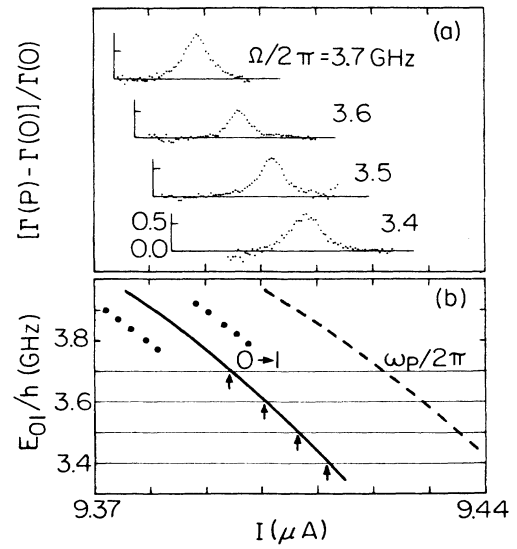

FIG. 18. (a) $[\Gamma(P)-\Gamma(0)]/\Gamma(0)$ vs I for the 10×10 μm^2 junction at 18 mK for four microwave frequencies. (b) Calculated energy level spacing E_{01} vs I for $I_0=9.489\pm0.007$ μA and $C=6.35\pm0.4$ pF. Dotted lines indicate uncertainties in E_{01} due to uncertainties in I_0 and C. Dashed line indicates the plasma frequency.

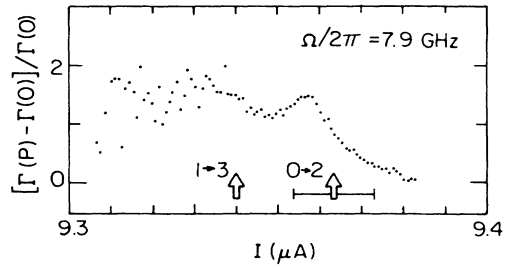

FIG. 19. $[\Gamma(P)-\Gamma(0)]/\Gamma(0)$ vs I for the junction of Fig. 18 with a microwave frequency of 7.9 GHz. Arrows indicate values of the bias current at which the calculated energy level spacings E_{02} and E_{13} equal $\hbar\Omega$. The error bar indicates the uncertainty of the $0\rightarrow2$ prediction due to the uncertainties in I_0 and C.

The positions of these peaks were compared with the energy-level predictions shown in Fig. 16(b). We measured $I_0=30.572\pm0.017$ μA from the current dependence of the escape rate at 28 mK. The capacitance was determined from the classical resonant activation measurements at 63 mK and 2.3 GHz and at 100 mK and 2.5 GHz, which yielded 46 and 48.5 pF, respectively: We adopted the value $C=47\pm3$ pF. The solid lines in Fig. 17(b) show the energy-level spacings $E_{n,n+1}/\hbar$ ($n=0,1,2$) versus I obtained from the energy-level calculations and the measured junction parameters. The intersection of the three curves with the horizontal line corresponding to the microwave frequency of 2.0 GHz predicts the bias current at which the resonant peaks should occur. The absolute positions of the measured peaks along the current axis agree with the predictions to within the experimental uncertainty. The dotted line indicates the uncertainty for the $0\rightarrow1$ transition: The error in energy arises from the uncertainty in C while that in current arises from the uncertainty in I_0 (and hence in $I-I_0$). A given error in I_0 or C shifts all three curves by very nearly the same amount. Thus, the *separations* of the measured peaks are in excellent agreement with the predicted separations.

In Fig. 18(a) we show data taken at 19 mK on the junc-

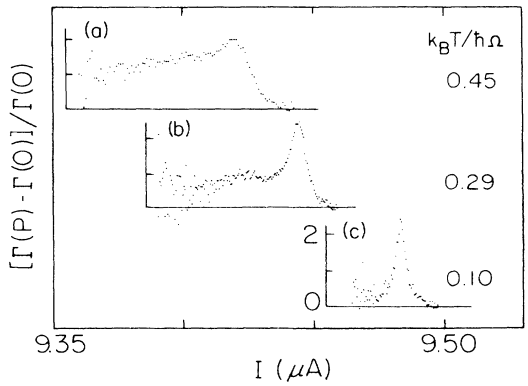

FIG. 20. $[\Gamma(P)-\Gamma(0)]/\Gamma(0)$ vs I for the junction of Fig. 18 with $I_0\approx9.57$ μA and $C\approx6.35$ pF at three values of $k_BT/\hbar\Omega$. The microwave frequencies are (a) 4.5 GHz, (b) 4.1 GHz, and (c) 3.7 GHz.

tion described in detail in Secs. IV and V. There are only two or three states in the well ($\Delta U/\hbar\omega_p \approx 2$) and the data are strongly in the quantum regime ($k_B T/\hbar\Omega \approx 0.1$). We plot the observed resonances for four different microwave frequencies. Only one peak is observed at each frequency since there is no significant population of the excited states. Figure 18(b) shows the predicted spacing between the ground state and the first excited states, together with the uncertainty. The absolute positions agree to within the uncertainty, which corresponds to an uncertainty in frequency of $\pm 3\%$. The shift in the current at which the resonances occur as the frequency is changed is in excellent agreement with the predicted shift. Furthermore, the measured frequencies of the resonances are clearly distinct from the classical (plasma) frequency of the particle at the bottom of the well, indicated by a dashed line.

Because of the anharmonic nature of the potential well, nonvanishing matrix elements $\langle i \mid \delta \mid f \rangle$ are expected, in particular, for $\mid i-f \mid = 2$; such transitions are strictly forbidden for the harmonic oscillator. In Fig. 19 we show an example of such a transition for the junction described in Fig. 18 with a microwave frequency of 7.9 GHz ($\approx \omega_p/\pi$) and at $T = 57$ mK. A well-defined resonance is clearly observed, perhaps with a second broad resonance at slightly lower currents. The predicted currents for the positions of the $0 \rightarrow 2$ and $1 \rightarrow 3$ transitions are shown with the open arrow; the error bar indicates the uncertainty of the position for both transitions due to the uncertainties in I_0 and C. The agreement between the positions of the observed and predicted $0 \rightarrow 2$ resonance is excellent.

As a final example, to illustrate the evolution from quantum to classical behavior in Fig. 20 we show the temperature dependence of the resonant response to microwaves for the junction studied in Fig. 18, with a critical current that was slightly higher because the data were obtained during a different run of the dilution refrigerator. The shape of the resonance changes markedly as $k_B T/\hbar\omega_p$ is increased. At the lowest temperature (c) at which the junction was firmly in the quantum regime, a single approximately Lorentzian-shaped resonance is observed. No other transitions appear because the thermal population of the excited states is negligible. At the intermediate temperature (b) a shoulder corresponding to the $1 \rightarrow 2$ transition appears, as a result of the nonnegligible thermal population of the first excited state. At the highest temperature (a) the resonance becomes broad and asymmetric: There are several closely spaced states in the well ($\Delta U/\hbar\omega_p \approx 4$) with substantial thermal population, and thus several transitions can occur. The individual transitions overlap to form a continuous response, that is characteristic of classical resonant activation (see Fig. 5).

B. Theory

We now describe a simple model for the effect of microwaves on the escape rate that enables us to predict the relative linewidths and strengths of the resonances. We first restrict ourselves to temperatures sufficiently high ($T > T_{cr}$) for the escape to be dominated by thermal activation, but sufficiently low for there to be only a few levels in the well, so that the level spacings are distinct; this is the case in Fig. 17. In the absence of microwaves the escape rate can be treated in terms of a series of thermally activated transitions between adjacent energy levels. We define the ratio of the population of the nth energy level to the $(n-1)$th energy level to be r_n. The escape rate can be written as an attempt frequency $\omega_p/2\pi$ multiplied by the occupancy of the state m at the top of the well:

$$\Gamma = \frac{\omega_p}{2\pi} \frac{1}{\eta} \prod_{n=1}^{m} r_n \ , \tag{6.1}$$

where the normalization factor η is given by

$$\eta = 1 + r_1 + r_1 r_2 + r_1 r_2 r_3 + \cdots + \prod_{n=1}^{m} r_n \ . \tag{6.2}$$

This result assumes that tunneling is negligible.

Replacing r_n by $\exp(-E_{n,n+1}/k_B T)$ we find

$$\Gamma = (\omega_p/2\pi)\exp[-(\Delta U - E_0)/k_B T] \ ,$$

which resembles Eq. (2.6) with $a_t = 1$, apart from the zero-point energy E_0. Since we are interested only in changes in escape rate, these discrepancies are not important.

We now calculate $\Gamma(P,\Omega)$, the escape rate in the presence of microwave radiation at frequency $\Omega/2\pi$. Since all the energy spacings are distinct, microwave-induced transitions for $\Omega \lesssim \omega_p$ occur only between two adjacent levels which we label i and f. Thus, the calculation of the enhancement $\gamma = \Gamma(P,\Omega)/\Gamma(0)$ is reduced to the calculation of the relative population $r_f(P,\Omega)$ when microwaves and thermal noise are both present. Since the microwave and thermal excitation processes add incoherently, we can use a detailed balance equation to find

$$r_f(P,\Omega) = \frac{R^T_{i\rightarrow f} + M_{i\rightarrow f}(P,\Omega)}{R^T_{f\rightarrow i} + M_{f\rightarrow i}(P,\Omega)} \ . \tag{6.3}$$

Here, $R^T_{i\rightarrow f}$ and $R^T_{f\rightarrow i}$ are the transition rates from the states i to f and f to i, respectively, induced by the thermal fluctuations of the resistor at temperature T. Similarly, $M_{i\rightarrow f}(P,\Omega)$ and $M_{f\rightarrow i}(P,\Omega)$ are the transition rates from the states i to f and f to i, respectively, induced by the microwave irradiation. In writing Eq. (6.3) we have neglected any coherence between levels induced by the microwaves.

Using $R^T_{i\rightarrow f}/R^T_{f\rightarrow i} = \exp(-E_{fi}/k_B T) = r_f$ and $M_{i\rightarrow f}(P,\Omega) = M_{f\rightarrow i}(P,\Omega)$, we rewrite Eq. (6.3) as

$$r_f(P,\Omega) = r_f \frac{1 + \rho_{fi}(P,\Omega)/r_f}{1 + \rho_{fi}(P,\Omega)} \ , \tag{6.4}$$

where

$$\rho_{fi}(P,\Omega) = M_{i\rightarrow f}(P,\Omega)/R^T_{f\rightarrow i} \ .$$

Combining Eqs. (6.1) and (6.4), and retaining terms that are first order in $M_{i\rightarrow f}(P,\Omega)$ and lowest order in r_f, we obtain

$$\gamma(P,\Omega) - 1 = \rho_{fi}(P,\Omega)/r_f \ . \tag{6.5}$$

The frequency dependence of ρ_{fi} arises from the frequency dependence of $M_{i\rightarrow f}(P,\Omega)$. From the theory of atomic

absorption spectra[36] one expects this dependence to be Lorentzian with a center frequency $E_{if}/\hbar$ and a full width at half height $W_{if}/\hbar$ given by $(\tau_i^{-1}+\tau_f^{-1})$, where τ_i and τ_f are the lifetimes of the states i and f.

In Ref. 26 we show that the lifetime of a state n in the well due to dissipation is given by

$$\tau_n^{-1}=2\sum_{l<n}\frac{|\langle n|\delta|l\rangle|^2}{R}E_{ln}/\hbar\ . \tag{6.6}$$

This result is derived under the assumption that the lifetime of the state is entirely due to the ground-state fluctuations of the resistor, and that thermal fluctuations of the resistor as well as tunneling out of the well are negligible. These two approximations are completely justified in the present context.

We now use the theory of atomic spectra to compute the integral

$$\int_0^\infty d\Omega\rho_{fi}(P,\Omega)$$

which is analogous to the ratio of the absorption and spontaneous emission coefficients. We finally obtain the complete expression

$$\rho_{fi}(P,\Omega)=\frac{P}{2E_{fi}}\frac{\left[\frac{\tau_f^{-1}+\tau_i^{-1}}{2}\right]}{\left[\Omega-\frac{E_{fi}}{\hbar}\right]^2+\left[\frac{\tau_f^{-1}+\tau_i^{-1}}{2}\right]^2}\ , \tag{6.7}$$

which, with Eq. (6.5), yields $\gamma(P,\Omega)$.

In the case where $T<T_{cr}$, that is quantum tunneling is the dominant escape mechanism as is the case for Fig. 18, a similar analysis can be carried out. One finds that Eqs. (6.5)–(6.7) can still be used to predict the shape of the resonance due to microwave induced transitions from the ground state to excited states, provided one replaces r_f by the ratio of tunneling rates out of the excited state and the ground state.

We now examine our experimental results in the light of these predictions. For the matrix elements for transitions between levels we take those of the harmonic oscillator; this approximation leads to an error of at most a few percent. Thus, we expect the resonance between the states i and f to have a Lorentzian line shape with a relative width

$$\frac{W_{if}}{E_{if}}\approx\frac{i+f}{Q}\ . \tag{6.8}$$

For example, the relative linewidth for the transition between the ground and first excited states is $W_{10}/E_{10}\approx 1/Q$. We convert the width of a resonance in current into a width in frequency using the measured dependence of the position of the peak on current.

The data in Fig. 18(a), which are in the limit $T<T_{cr}$, yield $E_{01}/W_{01}=50\pm10$. The value of Q measured with classical resonant activation is 30 ± 15; within the errors, the two values agree. For the $0\rightarrow2$ transition in Fig. 19 we used the width of the resonance on the high-current side to find $E_{02}/W_{02}=24\pm6$. This value is in good agreement with $E_{01}/2W_{01}$.

Finally, we discuss the relative widths and intensities of the transitions shown in Fig. 17, which are in the limit $T>T_{cr}$. Since the transitions are measured at constant microwave frequency, the relative linewidths should scale as $W_{01}:W_{12}:W_{23}\approx 1:3:5$. Furthermore, the intensity of each Lorentzian linewidth [Eq. (6.7)] integrated over frequency, is the same for all transitions. We note also that the exponential term r_f in Eq. (6.5) is constant because the microwave frequency is the same for all transitions. In Fig. 21 we have plotted the predicted line shapes for the data of Fig. 17, obtained by adding ρ_{fi}/Γ_f of the three Lorentzians. The absolute position, width, and height of the $0\rightarrow1$ resonance were fitted to a Lorentzian with $Q\approx75$, and these values used to predict the widths transition is well fitted by a Lorentzian line shape. For the $1\rightarrow2$ transition the predicted width is in quite good agreement with experiment, although the height is about 30% low. The measured $2\rightarrow3$ transition is very smeared out, but its width and height are at least consistent with the predictions. Given the simplicity of the model, we feel that the fit of the theory to the experiment is quite good.

VII. CONCLUDING SUMMARY

We have described experiments demonstrating the quantum mechanical behavior of a macroscopic degree of freedom, namely the phase difference δ across a current-biased Josephson junction. The relevant parameters entering the equations of motion were measured *in situ* using classical phenomena. These parameters are, first, the critical current, which determines the energy scale of the potential well, and, second, the admittance loading the junction, which determines both the "mass" associated with the motion of δ (capacitive part) and the damping of this motion (resistive part).

The critical current I_0, which was determined from the current dependence of the escape rate in the thermal regime, is required to high precision: In fact, the errors in the quantum measurements were dominated by the uncertainties in I_0. The accuracy with which I_0 is determined is limited partly by the uncertainty in Q used to make the correction for the departure of the thermal prefactor a_t from unity, and partly by the question of the precise value of α in a_t [Eq. (2.7)]. The fact that the inclusion of the prefactor correction yields a temperature-dependent critical current supports the form of a_t derived by Buttiker *et al.*[22] It is noteworthy that this experiment is accurate

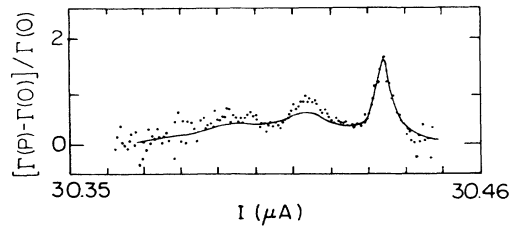

FIG. 21. $[\Gamma(P)-\Gamma(0)]/\Gamma(0)$ vs I for the data of Fig. 17 with the predicted lineshapes indicated by the solid line. The position, width, and height of the $0\rightarrow1$ transition is fitted.

enough to make prefactor corrections clearly discernible. Thus there is a need for further theoretical work on the classical prefactor, as well as on quantum corrections to the prefactor at temperatures not too far above T_{cr}.

The admittance loading the junction was determined in the vicinity of the plasma frequency from the current dependence of the enhancement of the thermal escape rate in the presence of microwaves. Our results show that to a first approximation the admittance can be modeled as a resistance in parallel with a capacitance. Most of this capacitance is contributed by the self-capacitance of the junction, while the resistance is dominated by the loading of the bias circuitry. The imperfections of the simple model are apparent in the frequency dependence of both the capacitance and the resistance. The model is adequate only because the capacitance variations are small compared with the junction capacitance, and Q is sufficiently large for the effects of dissipation on the escape rate to be almost negligible. We note that the resistively shunted junction model is likely to be inadequate for junctions with a smaller capacitance (say <1 pF) or for unshunted junctions with a Q small enough (say <5) for its reduction of the tunneling rate to be significant. The development of an improved type of mount with an admittance that varied less with frequency would be a major step forward. At the same time, although the effects of an arbitrary admittance on the MQT rate at $T=0$ have been calculated, the extension of these calculations to nonzero temperatures and to the classical regime would be most useful.

In the first series of experiments we measured the escape rate out of the zero-voltage state, expressing the results as an escape temperature T_{esc}. With the critical current at its maximum value, we observed that T_{esc} flattened off at low temperatures. Within the experimental uncertainties this low temperature value of T_{esc} was in excellent agreement with the predicted value at $T=0$, with all the necessary parameters measured *in situ* in the classical regime. When the critical current was reduced by a magnetic field, T_{esc} was nearly equal to the predicted value 0.95 T down to the lowest temperature of the experiment, indicating that spurious noise was negligible. Thus, we are confident that the flattening of T_{esc} for the high value of I_0 arose from MQT, that is, from the quantum mechanical broadening of δ. In these measurements, the effects of dissipation were almost negligible.

In the second series of experiments we measured the microwave-induced enhancement of the escape rate for two junctions in the quantum regime. The discrete Lorentzian-shaped resonances observed as a function of bias current [Fig. 17(a)] are characteristic of transitions between quantized energy levels in the well. The fact that these resonances occur at different values of current for the same microwave frequency is a consequence of the anharmonic nature of the potential well. The position of these resonances along the current axis and also the current dependence of the $0\rightarrow1$ transition for different microwave frequencies are in excellent agreement with predictions. Furthermore, the relative heights and widths of the constant-frequency resonances were in reasonable agreement with a simple quantum-mechanical calculation. The observation of these resonances provides a second, independent confirmation of the quantum nature of δ.

ACKNOWLEDGMENTS

We are indebted to D. Esteve, R. Landauer, and A. J. Leggett for helpful discussions, and to P. Hänggi for drawing our attention to Ref. 23. We thank K. Daley, S. Diamond, D. Esteve, R. E. Packard, N. E. Phillips, C. Urbina, J. Van Curen, and especially H. J. Mamin for advice on or assistance with the construction of our dilution refrigerator. J.M.M. gratefully acknowledges the support of the NSF and of IBM during the course of this work. J.C. would like to thank the members of Centre d'Etudes Nucleaires de Saclay, for their hospitality during the preparation of this manuscript. We acknowledge the use of the Microelectronics Facility in the Electronics Research Laboratory of the Electrical Engineering and Computer Science Department, University of California, Berkeley. This work was supported by the Director, Office of Energy Research, Office of Basic Energy Sciences, Materials Sciences Division of the U.S. Department of Energy under Contract No. DE-AC03-76SF00098, and by the Commissariat a' l'Energie Atomique (MHD).

*Present address: Service de Physique du Solide, Centre d'Etudes Nucleaires de Saclay, F-91191, Gif-sur-Yvette Cedex, France.

[1]A. J. Leggett, Prog. Theor. Phys. (Suppl.) **69**, 80 (1980); Contemp. Phys. **25**, 583 (1984); J. Phys. (Paris) Colloq. **39**, C6-1264 (1980); *Essays in Theoretical Physics in Honour of Dirk Ter Haar* (Pergamon, Oxford, 1984), p. 95.

[2]B. D. Josephson, Phys. Lett. **1**, 251 (1962); Adv. Phys. **14**, 419 (1965).

[3]Yu. M. Ivanchenko and L. A. Zilberman, Zh. Eksp. Teor. Fiz. **55**, 2395 (1968) [Sov. Phys.—JETP **28**, 1272 (1969)].

[4]A. O. Caldeira and A. J. Leggett, Ann. Phys. (N.Y.) **149**, 374 (1983).

[5]A. J. Leggett, in *Lecture Notes, Les Houches Summer School on Chance and Matter,* edited by J. Souletie, R. Stora, and J. Vannimenus (North-Holland, Amsterdam, 1986); P. Hänggi, J. Stat. Phys. **42**, 105 (1986); H. Grabert, in *Superconducting Quantum Interference Devices and their Applications,* edited by H. D. Hahlbohm and H. Lübbig (Walter de Gruyter, Berlin, 1985), p. 289.

[6]R. V. Voss and R. A. Webb, Phys. Rev. Lett. **47**, 265 (1981).

[7]L. D. Jackel, J. P. Gordon, E. L. Hu, R. E. Howard, L. A. Fetter, D. M. Tennant, R. W. Epworth, and J. Kurkijarvi, Phys. Rev. Lett. **47**, 697 (1981).

[8]W. den Boer and R. de Bruyn Ouboter, Physica **98B**, 185 (1980); D. W. Bol, R. van Weelderen, and R. de Bruyn Ouboter, *ibid.* **122B**, 2 (1983); D. W. Bol, J. J. F. Scheffer, W. T. Giele and R. de Bruyn Ouboter, *ibid.* **133B**, 196 (1985).

[9]R. J. Prance, A. P. Long, T. D. Clarke, A. Widom, J. E. Mutton, J. Sacco, M. W. Potts, G. Megaloudis, and F. Goodall, Nature **289**, 543 (1981).

[10]I. M. Dmitrenko, V. A. Khlus, G. M. Tsoi, and V. I. Shnyrkov, Fiz. Nizk. Temp. **11**, 146 (1985) [Sov. J. Low. Temp. Phys. **11**, 77 (1985)].

[11]S. Washburn, R. A. Webb, R. F. Voss, and S. M. Faris, Phys. Rev. Lett. **54**, 2712 (1985).

[12]D. B. Schwartz, B. Sen, C. N. Archie, and J. E. Lukens, Phys. Rev. Lett. **55**, 1547 (1985).

[13]H. Grabert, P. Olschowski, and U. Weiss, Phys. Rev. B **32**, 3348 (1985).

[14]H. Grabert, P. Olschowski, and U. Weiss, Phys. Rev. Lett. **57**, 265 (1986); D. B. Schwartz, B. Sen, C. N. Archie, and J. E. Lukens, *ibid.* **57**, 266 (1986).

[15]M. H. Devoret, J. M. Martinis, D. Esteve, and J. Clarke, Phys. Rev. Lett. **53**, 1260 (1984).

[16]J. M. Martinis, M. H. Devoret, and J. Clarke, Phys. Rev. Lett. **55**, 1543 (1985).

[17]M. H. Devoret, J. M. Martinis, and J. Clarke, Phys. Rev. Lett. **55**, 1908 (1985).

[18]J. M. Martinis, Ph.D. thesis, University of California, Berkeley, LBL Report No. 20803, 1985.

[19]V. Ambegaokar, U. Eckern, and G. Schön, Phys. Rev. Lett. **48**, 1745 (1982); U. Eckern, G. Schön, and V. Ambegaokar, Phys. Rev. B **30**, 6419 (1984); A. I. Larkin and Yu. N. Ovchinnikov, *ibid.* **28**, 6281 (1983).

[20]T. A. Fulton and L. N. Dunkleberger, Phys. Rev. B **9**, 4760 (1974).

[21]H. A. Kramers, Physica (Utrecht) **7**, 284 (1940).

[22]M. Büttiker, E. P. Harris, and R. Landauer, Phys. Rev. B **28**, 1268 (1983).

[23]H. Risken and K. Voigtlaender, J. Stat. Phys. **41**, 825 (1985).

[24]It can be shown that the use of the exact expression for the potential in the WKB calculation rather than the cubic approximation leads to the tunneling exponent $-7.2(\Delta U/\hbar\omega_p)[1+0.052(1-I/I_0)+\cdots]$, where ΔU is given by Eq. (2.3). For the experiments reported in this paper, I/I_0 is very close to one and the error due to our use of the cubic approximation is totally negligible.

[25]A. J. Leggett, Phys. Rev. B **30**, 1208 (1984).

[26]D. Esteve, M. H. Devoret, and J. M. Martinis, Phys. Rev. B **34**, 158 (1986).

[27]S. Chakravarty and A. Schmid, Phys. Rev. B **33**, 2000 (1986).

[28]V. I. Gol'danskii, Dokl. Akad. Nauk SSSR **124**, 1261 (1959); I. Affleck, Phys. Rev. Lett. **46**, 388 (1981).

[29]H. Grabert and U. Weiss, Phys. Rev. Lett. **53**, 1787 (1984); P. Hänggi, H. Grabert, G. L. Ingold, and U. Weiss, *ibid.* **55**, 761 (1985).

[30]The derivation of Eqs. (2.10) and (2.11) assumes a Boltzmann population of the states in the well, thereby ignoring the depletion of the states near the top of the well that enters into Eq. (2.7).

[31]M. H. Devoret, J. M. Martinis, A. N. Cleland, J. Clarke, and D. Esteve (unpublished).

[32]T. Fonseca and P. Grignolini, Phys. Rev. A **33**, 122 (1986).

[33]B. I. Ivlev and V. I. Mel'nikov (unpublished).

[34]A. I. Larkin and Yu. N. Ovchinnikov, J. Low Temp. Phys. **63**, 317 (1986).

[35]P is defined as the microwave power, at a particular frequency, absorbed by the shunt resistance R in the absence of the junction.

[36]W. Heitler, *The Quantum Theory of Radiation*, 3rd ed. (Oxford University Press, Oxford, 1954).